# A Theoretical Omega-Square Model Considering the Spatial Variation in Slip and Rupture Velocity

by Yoshiaki Hisada

**Abstract**   A theoretical model for constructing the $\omega$-squared model is proposed by modifying the $k$-squared model of Bernard *et al.* (1996). The $k$-squared model provides a theoretical basis for the empirical $\omega$-squared model under the assumptions that (1) the spatial wavenumber spectrum of the slip distribution falls off as the inverse of the wavenumber squared ($k$-squared), (2) the Fourier amplitudes of the slip velocity are independent of $\omega$ at high frequencies, and (3) the rupture velocity is constant. In this study, a more realistic model is proposed by modifying the last two assumptions. First, a Kostrov-type slip velocity model is proposed by superposing equilateral triangles, in which a source-controlled *fmax* is imposed by the minimum duration among the triangles. The Fourier amplitude of our slip velocity model falls off as the inverse of $\omega$ at high frequencies less than *fmax*. Next, in order to model variable rupture velocities, the incoherent rupture time ($\Delta t_r$), namely, the difference between the actual rupture time and the coherent (average) rupture time, is introduced. After checking various models for $\Delta t_r$ distributions, the $k$-squared model for $\Delta t_r$, similar to that for the slip distributions of the $k$-squared model, is found to be the most plausible. Finally, it is confirmed that the proposed source model (we call it as the $\omega$-inverse-squared model), which consists of the combination of the slip velocity proposed here and the $k$-squared distributions for both slip and $\Delta t_r$, not only is consistent with the empirical $\omega$-squared model, but also provides the theoretical basis for constructing realistic source models at broadband frequencies.

## Introduction

Since the pioneering work of Aki (1967) to construct the scaling law of seismic source spectra, the $\omega$-squared model has been the most widely used empirical tool for predicting strong ground motions (e.g., Aki, 1972; Hanks, 1979; Hanks and McGuire, 1981; Boore, 1983; Joyner, 1984; Irikura, 1986). Originally, its spectrum was rather simple, with one or two corner frequencies corresponding to the fault dimension and/or the rise time using smooth and homogeneous faulting models (Haskell, 1964; Kostrov, 1964; Brune, 1970; Madariaga, 1976). Later, a cut-off frequency, *fmax,* was introduced to reproduce the steep falloff of the observational spectra at higher frequencies (Hanks, 1979, 1982). On the other hand, observational and numerical results have shown that earthquake source processes are highly heterogeneous. Thus, barrier/asperity models were proposed to include the added complexities (Das and Aki, 1977; Kanamori and Stewart, 1978; Mikumo and Miyatake, 1978; Boatwright, 1982). Subsequently, the $\omega$-squared model has been modified by including the so-called patch corner frequencies, which correspond to the barrier/asperity size (e.g., Gusev, 1983; Papageorgiou and Aki, 1983; Koyama, 1985).

Recently, Herrero and Bernard (1994) and Bernard *et al.* (1996) proposed the $k$-squared model as a theoretical $\omega$-squared model. The main assumption of this model is that the spatial wavenumber spectrum of the final slip distribution falls off as the inverse of the wavenumber squared ($k$-squared). This model yields a stress drop independent of seismic moment, which is consistent with the stochastic model of Andrews (1981) and the fractal model of Frankel (1991) with the fractal dimension of 2. In addition, Somerville *et al.* (1999) found that slip distributions derived from source inversion studies using strong motion records are consistent with the $k$-squared model up to about 1 Hz. The $k$-squared model is also consistent with the $\omega$-squared model under the assumptions of constant rupture velocity and scale-dependent rise time (Bernard *et al.,* 1996). However, the actual rupture velocity probably fluctuates significantly in realistic situations (Das and Aki, 1977; Mikumo and Miyatake, 1978; Archuleta, 1982). Since the fluctuation of the rupture front excites strong high-frequency waves (e.g., Madariaga, 1977), the $k$-squared model should be modified in order to construct a more realistic $\omega$-squared model.

The purpose of this study is to propose a theoretical $\omega$-squared model. For this, we will modify the $k$-squared model

of Bernard *et al.* (1996) by considering realistic spatial variations in both slip and rupture velocities. This article consists of five sections. First, I show the formulation of the far-field displacement using a unilateral source model. Second, I briefly review the formulation of the *k*-squared model. Third, I propose a realistic and practical slip velocity model by considering the results from dynamic source modelings and laboratory experiments. Fourth, I introduce the effects of the variable rupture velocities in the model using the incoherent rupture time. Finally, I propose a "omega-inverse-squared model" for constructing the $\omega$-squared model, and discuss its characteristics in comparison with the *k*-squared model and the empirical $\omega$-squared model.

## Source Spectra for Far-Field Displacements

Following Bernard *et al.* (1996), I consider a 1-D fault model with unilateral rupture propagation, embedded in a homogeneous full-space (Fig. 1). The far-field displacements, $U_i$, at a station *Y* from this source model can be written as

$$U_i(Y; \omega) = \frac{R_i}{4\pi\rho r c^3} M_o(\omega), \qquad (1)$$

where $\omega$ is the circular frequency, the subscript *i* denotes the *i*th component in the spherical coordinate system, and $R_i$ is the radiation pattern for the *i*th component. The variable *c* is the medium velocity ($V_P$ for the radial, and $V_S$ for the transverse and vertical directions), $\rho$ is the density, and *r* is the distance from the rupture front, *x*, to *Y*. $M_o$ in equation (1) is the source spectrum (e.g., Dan and Sato, 1999), and is expressed as

$$M_o(\omega) = \mu W \int_0^L V(x; \omega) \exp\{i\omega(t_c + t_r)\}dx, \quad (2)$$

where, $\mu$ is the rigidity, *V* is the Fourier transform of the slip velocity at a specific point *x* on the fault plane, and *W* and *L* are the width and length of the fault, respectively. In equation (2), $t_c$ and $t_r$ are the arrival time of the seismic waves and the rupture time, respectively, and are given as follows:

$$t_c = \frac{r}{c} \approx \frac{r_0 - x \cdot \cos\theta}{c}, \ (x \ll r_0) \qquad (3)$$

and,

$$t_r = \frac{x}{\bar{V}r} + \Delta t_r(x). \qquad (4)$$

where, $r_0$ is the distance from the origin of the rupture front to *Y*, $\theta$ is the angle between the directions of the rupture propagation and the seismic waves, and $\bar{V}_r$ is the average rupture velocity. As shown in equation (4), I divide the rup-
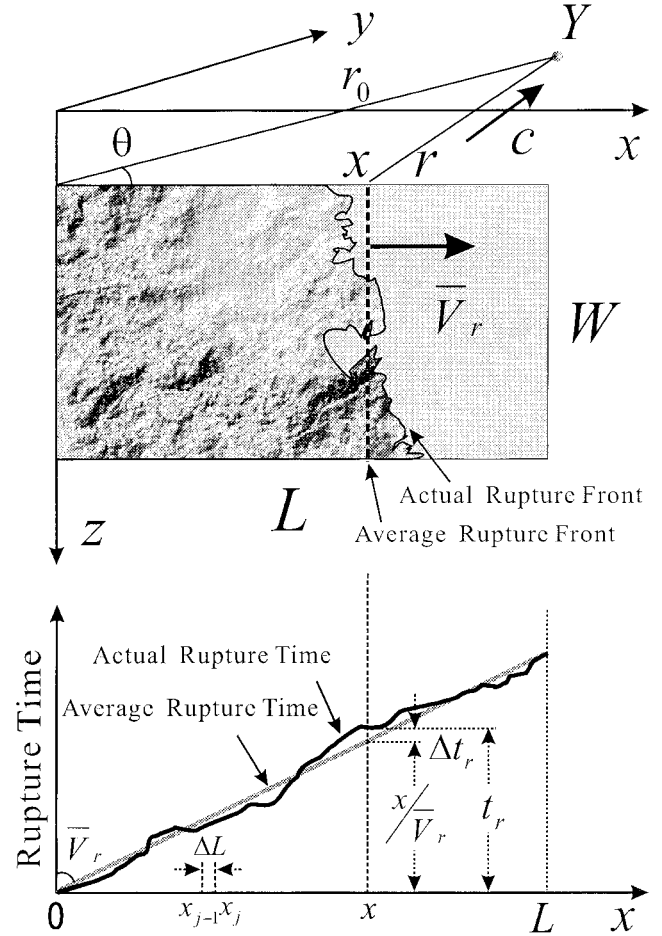


Figure 1.   Geometry of a unilateral source and an observation station in the far-field (top), and modeling of variable rupture time using the incoherent rupture time $\Delta t$ (bottom).

ture time $t_r$ into the coherent (average) rupture time and the incoherent rupture time $\Delta t_r$. I introduce $\Delta t_r$ to include the effects of fluctuations at the rupture front (see Figure 1). For convenience, I express the slip velocity function *V* by the product of the slip (dislocation) and the slip velocity function of the unit dislocation.

$$V(x; \omega) = D(x)F_V(x; \omega) \qquad (5)$$

Substituting equations (3), (4), and (5) into equation (2), I obtain the following source spectra,

$$M_o(\omega) = \mu W \exp(i\omega r_o/c)\int_0^L D(x)F_V(x; \omega)$$
$$\exp\left\{i\omega\left(\frac{x}{\bar{V}_r C_d} + \Delta t_r\right)\right\}dx, \qquad (6)$$

where, $C_d$ is the directivity coefficient (Ben-Menahem, 1961),

$$C_d = \frac{1}{1 - \dfrac{Vr}{c} \cdot \cos\theta}. \tag{7}$$

## K-Squared Model with Scale-Dependent Rise Time

Here I briefly explain the *k*-squared model (Herrero and Bernard, 1994; Bernard *et al.,* 1996) and discuss some physical problems that suggest the need to modify this model.

The main assumptions for the *k*-squared model are as follows:

a. The Fourier amplitudes of spatial wavenumber (*k*) spectra of the slip distribution *D* decay as $k^{-2}$.
b. The slip velocity function $F_V$ is the rectangular boxcar whose rise time is inversely proportional to wavenumber (or frequency) at high frequencies. This assures frequency-independent Fourier amplitudes of $F_V$, as will be shown below.
c. The rupture velocity $V_r$ is constant, namely $\Delta t_r = 0$ in equation (6).

Assumption (a) is based on the self-similarity of the spatial distribution of the slip, and this explains a stress drop independent of seismic moment and fault size. Assumptions (b) and (c) were introduced to produce the $\omega$-squared model. Regarding assumption (b), Herrero and Bernard (1994) originally adopted the delta function (instantaneous slip), but later Bernard *et al.* (1996) used the rectangular boxcar with the scale-dependent (or, frequency-dependent) rise time. The slip-velocity function $F_V$ of the boxcar can be expressed as follows,

$$F_V(x;\omega) = \frac{\sin\chi_\tau}{\chi_\tau} e^{i\chi_\tau}, \tag{8}$$

$$\text{where, } \chi_\tau = \frac{\omega\tau(x;\omega)}{2} \tag{9}$$

Using assumption (b), the rise time $\tau$ is inversely proportional to $\omega$ (or wavenumber) at high frequencies, as follows,

$$\tau(x;\omega) = \begin{cases} \tau_{max}, & (\omega \le 2\pi aC_d/\tau_{max}) \\ \dfrac{2\pi aC_d}{\omega}, & (\omega \ge 2\pi aC_d/\tau_{max}) \end{cases} \tag{10}$$

$$\text{with } \tau_{max} = L_0/\bar{V}_r$$

where $\tau_{max}$ is the total slip duration at *x,* and $L_0$ is some characteristic dimension representing the barrier/asperity size. A nondimensional coefficient, *a,* is the ratio of the local rise time over the propagation time of the average rupture front along a wavelength (Bernard *et al.,* 1996); this coefficient was introduced to incorporate the observed short slip duration (Heaton, 1990).

Substituting equations (8), (9), and (10) into equation (6), and changing the bounds of the integration, the source spectrum can be expressed as:

$$M_o(\omega) \tag{11}$$
$$= \mu W \overline{F_V} \exp(i\omega r_o/c)\int_{-\infty}^{+\infty} D(x) \exp(2\pi ikx)dx,$$

$$\text{with } k = \frac{\omega}{2\pi C_d\bar{V}_r} = \frac{f}{C_d\bar{V}_r}, \tag{12}$$

$$\text{and } \overline{F_V}(f) = \begin{cases} \dfrac{\sin(\pi f\tau_{max})}{\pi f\tau_{max}}, & (f \le f_0) \\ \dfrac{\sin\,(\pi aC_d)}{\pi aC_d}, & (f \ge f_0) \end{cases} \tag{13}$$

$$\text{with } f_0 = aC_d/\tau_{max}$$

The spectrum amplitudes of slip velocity function (equation [13]) are independent of frequency for frequencies greater than $f_0$. It should be noted that equation (13) can lead to unrealistic results for $aC_d = 1$; $\overline{F_V}$ is zero for $f \ge f_0$.

The integration in equation (11) is the Fourier transform of the slip distribution with respect to the wavenumber. Under assumption (a), Herrero and Bernard (1994) proposed the following integrand:

$$\int_{-\infty}^{+\infty} D(x) \exp(2\pi ikx)dx = \bar{D}L\,F_{ph}(k)$$
$$\times \begin{cases} 1, & (k \le 1/L) \\ \dfrac{1}{(kL)^2}, & (k \ge 1/L) \end{cases} \tag{14}$$

where $\bar{D}$ is the average slip over the fault plane, and $F_{ph}$ is a phase function with unit amplitude.

Finally, the source spectrum of the *k*-squared model is obtained by substituting equations (12) and (14) into (11). Using frequency *f* instead of $\omega$, the source spectrum can be expressed as

$$M_o(f) = \overline{M_0}\,\overline{F_V}\,\exp(2\pi fir_o/c)F_{ph}(f)$$
$$\times \begin{cases} 1, & (f \le f_C) \\ \left(\dfrac{f_C}{f}\right)^2, & (f \ge f_C) \end{cases}, \text{ with } f_C = \frac{\bar{V}_rC_d}{L} \tag{15}$$

where $\overline{M_0}$ is the seismic moment ($= \mu\bar{D}LW$; $\bar{D}$ is the average slip). Combining equations (13) and (15), the *k*-squared model yields the $\omega$-squared model with two corner frequencies ($f_0$ and $f_C$: usually $f_0 > f_C$).

On the other hand, the *k*-squared model is based on two physically unrealistic assumptions: (1) the boxcar model for the slip velocity, and (2) a constant rupture velocity. The Fourier amplitude of a boxcar falls off as the inverse of $\omega$, and generates infinite slip accelerations at the starting and

stopping phases. To produce finite accelerations, smoother slip velocities have to be used, such as a combination of triangles as used for source inversion studies. Since the Fourier amplitudes of triangles fall off as the inverse of $\omega$-squared, it is difficult to model the amplitudes of slip velocity as being independent of $\omega$. Consequently, the variable rupture velocity should be incorporated to excite high-frequency waves. Next, I investigate the effects of a more realistic slip velocity, together with a variable rupture velocity.

## Modification of K-Squared Model Considering Realistic Slip Velocity and Variable Rupture Velocity

### Fourier Amplitude Spectra of a Realistic Slip Velocity Function

An analytic solution for the slip velocity was derived by Kostrov (1964) using a self-similar circular crack. Its amplitude in time history is infinite at the crack tip, and falls off as the inverse of a square root of time. More realistically, dynamic source modeling and laboratory experiments on rock indicate that the slip velocity exhibits a sharp rise with a finite amplitude and is followed by a relatively smooth decay (e.g., Madariaga, 1976, 1977; Day, 1982; Ohnaka and Kuwahara, 1990; Miyatake, 1998). The finiteness of the velocity amplitude at the crack tip is probably caused by non-linear breakdown processes, such as local yielding (e.g., Madariaga, 1977). Accordingly, it may cause the source-controlled $f_{\max}$ (Papageorgiou and Aki, 1983).

In order to construct the realistic slip velocity functions, I adopt a simple and practical model. As shown in Figure 2, I construct the slip velocity function $f_v$ by superimposing equilateral triangles with different durations. In the time domain, it can be written as follows;

$$f_v(x; t) = \frac{1}{A} \sum_{j=1}^{N_V} A_r^{j-1} \dot{f}_j(x; t) \quad \text{with } A = \sum_{j=1}^{N_V} A_r^{j-1}, \quad (16)$$

where $N_V$ is the total number of the triangles, $Ar$ is the ratio of the area of the $j$th triangle with respect to the area of the $j-1$th triangle.

In equation (16), $\dot{f}_j$ is the equilateral triangle of the $j$th element,

$$\dot{f}_j(x; t) = \begin{cases} A_j t, & (t \leq \tau_j/2) \\ A_j(\tau_j - t), & (\tau_j/2 \leq t \leq \tau_j) \\ 0, & (\tau_j \leq l) \end{cases} \quad (17)$$

$$\text{with } A_j = 2V_j/\tau_j, \quad \text{and } V_j = 2/\tau_j. \quad (18)$$

$A_j$ and $V_j$ are the maximum acceleration and velocity of the $j$th triangle, respectively. $\tau_j$ is the duration of the $j$th triangle, and I adopt here the following values,

$$\tau_j = \frac{2^{j-1}}{f_{\max}}, \quad \text{with } \tau_{\min} \equiv \tau_1 = \frac{1}{f_{\max}}, \quad (19)$$

$$\text{and } \tau_{\max} \equiv \tau N_v, = \frac{2^{N_v - 1}}{f_{\max}}$$

where I use a coefficient of the $j$-1th power of 2 to avoid the artificial peaks and troughs not only in the time domain (see Figure 2), but also in the frequency domain (Fig. 3). Note that, the reciprocal of the minimum duration ($\tau_1$) gives a source-controlled $f_{\max}$ as shown subsequently. $\tau_{\max}$ is the total duration of the slip, which would be controlled by the characteristic size of barrier/asperity and/or the healing front (Heaton, 1990).

The slip displacement and acceleration functions are easily obtained by replacing $\dot{f}_j$ in equation (16) by

$$f_j(x; t)$$
$$= \begin{cases} 2(t/\tau_j)^2, & (t \leq \tau_j/2) \\ 0.5\{1 + (2t - \tau_j)(3\tau_j - 2t)/\tau_j^2\} & (\tau_j/2 \leq t \leq \tau_j), \\ 1, & (\tau_j \leq t) \end{cases}$$
$$(20)$$

for displacement, and

$$\ddot{f}_j(x; t) = \begin{cases} A_j, & (t \leq \tau_j/2) \\ -A_j, & (\tau_j/2 \leq t \leq \tau_j) \\ 0, & (\tau_j \leq t) \end{cases} \quad (21)$$

for acceleration.

Figure 2 shows examples for slip velocities and displacements in the following four cases, for $fmax = 10$ Hz ($\tau_1 = 0.1$ sec),

Case (A) $N_V = 3$ and $Ar = 1.0$,
Case (B) $N_V = 3$ and $Ar = \sqrt{2}$
Case (C) $N_V = 5$ and $Ar = 1.0$,
Case (D) $N_V = 5$ and $Ar = \sqrt{2}$.

The total slip durations ($\tau_{\max}$) for $N_V = 3$ and 5 are 0.4 and 1.6 seconds, respectively. The velocity for the smaller $N_V$ and $Ar$ shows the sharper and larger peak velocity. The velocities for $Ar = \sqrt{2}$ decay as $1/\sqrt{t}$, which is consistent with Kostrov's slip velocity. Although it is not shown, the slip velocity for $Ar = 2$ is a scalene triangle, which seems unrealistic as compared with the Kostrov-type slip velocity. On the other hand, results for $Ar < 1.0$ show unrealistically large slip velocities and accelerations for $f_{\max} = 10$ Hz. Thus, $Ar$ probably should take a value between 1 and 2.

The Fourier transform of equation (16) can be obtained analytically:

$$F_v(x; \omega) = \frac{1}{A} \sum_{j=1}^{N_v} A_r^{j-1} \left\{ \frac{\sin \chi_j}{\chi_j} \exp(i\chi_j) \right\}^2, \quad (22)$$

$$\text{and } \chi_j = \frac{\omega \tau_j}{4}$$
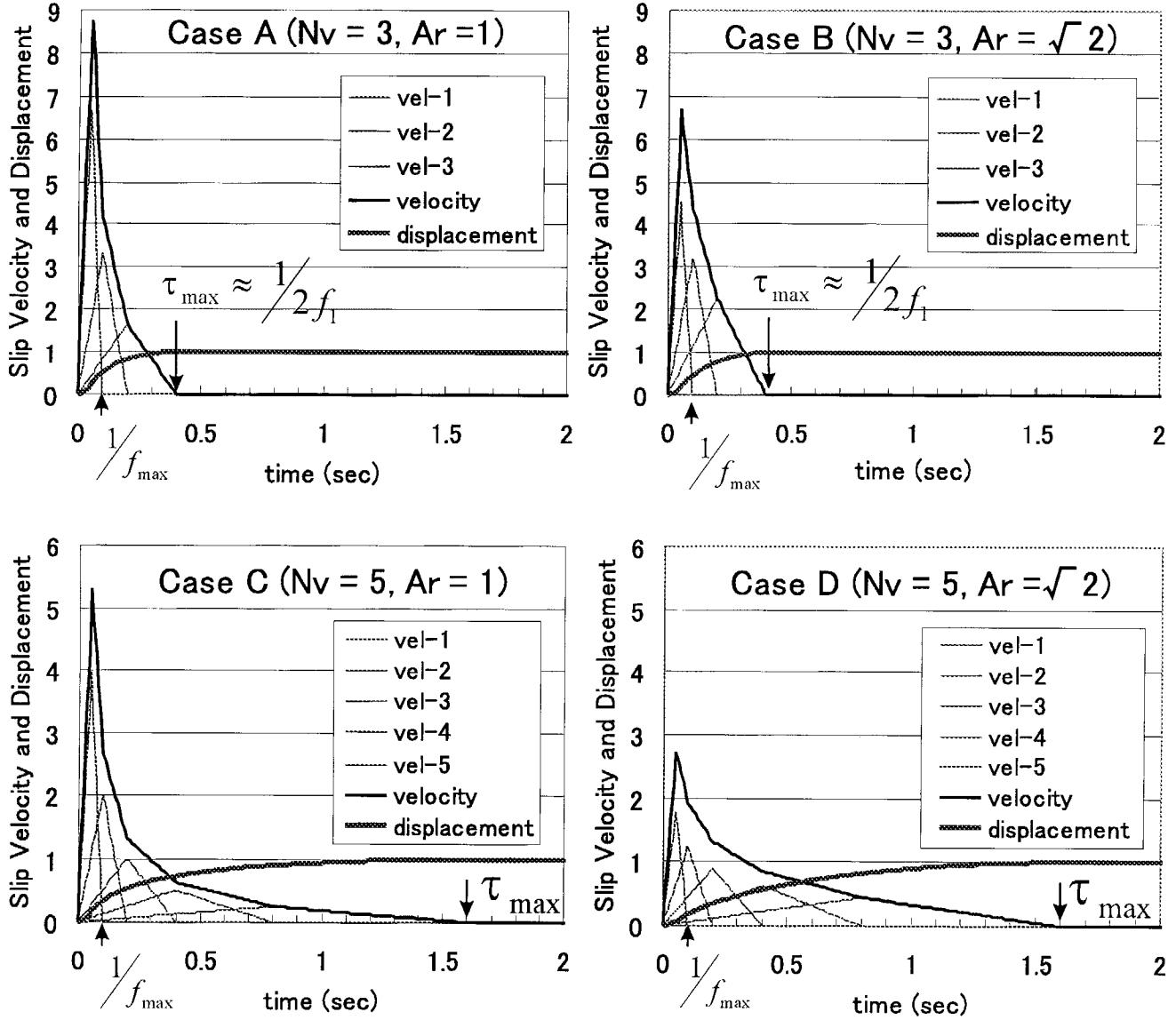
Figure 2. The slip velocities (thick black lines) and displacements (thick gray lines) for four cases. The slip velocities consist of equilateral triangles with different durations (thin lines). The reciprocal of the minimum duration among triangles generates the source-controlled $f_{max}$. The maximum duration $\tau_{max}$ among triangles equals to the total slip duration at a point on a fault plane, and the reciprocal of the double of $\tau_{max}$ is nearly equal to the first corner frequency $f_1$ (see Fig. 3).

Note that the Fourier amplitude of each triangle has an $\omega^{-2}$ decay.

Figure 3 shows the Fourier amplitudes of the slip velocities and accelerations corresponding to those in Figure 2. The amplitudes of all the slip velocities have two corner frequencies; $f_1 \approx 1/2\tau_{max}$ and $f_{max}$. The spectra are constant for frequencies lower than $f_1$, fall off as the inverse of $\omega$ between $f_1$ and $f_{max}$ and then fall off as the inverse of $\omega$-squared at frequencies greater than $f_{max}$. It is easy to control the spectrum shape and amplitude by changing these frequencies. In addition, the spectra do not exhibit artificial

sharp peaks and troughs at frequencies lower than $f_{max}$, which would be advantageous for predicting strong motions.

### Source Spectra Considering Variable Rupture Velocity

To investigate the effect of the variable rupture velocity on the source spectra, I evaluate the source spectra for $\Delta t_r \neq 0$, by assuming temporarily the instantaneous slip ($F_V(x, \omega) = 1$) in equation (6). The source spectra can be

$$S(\omega) = \int_0^L D(x) \exp\left\{i\omega\left(\frac{x}{V_r C_d} + \Delta t_r\right)\right\} dx. \quad (23)$$
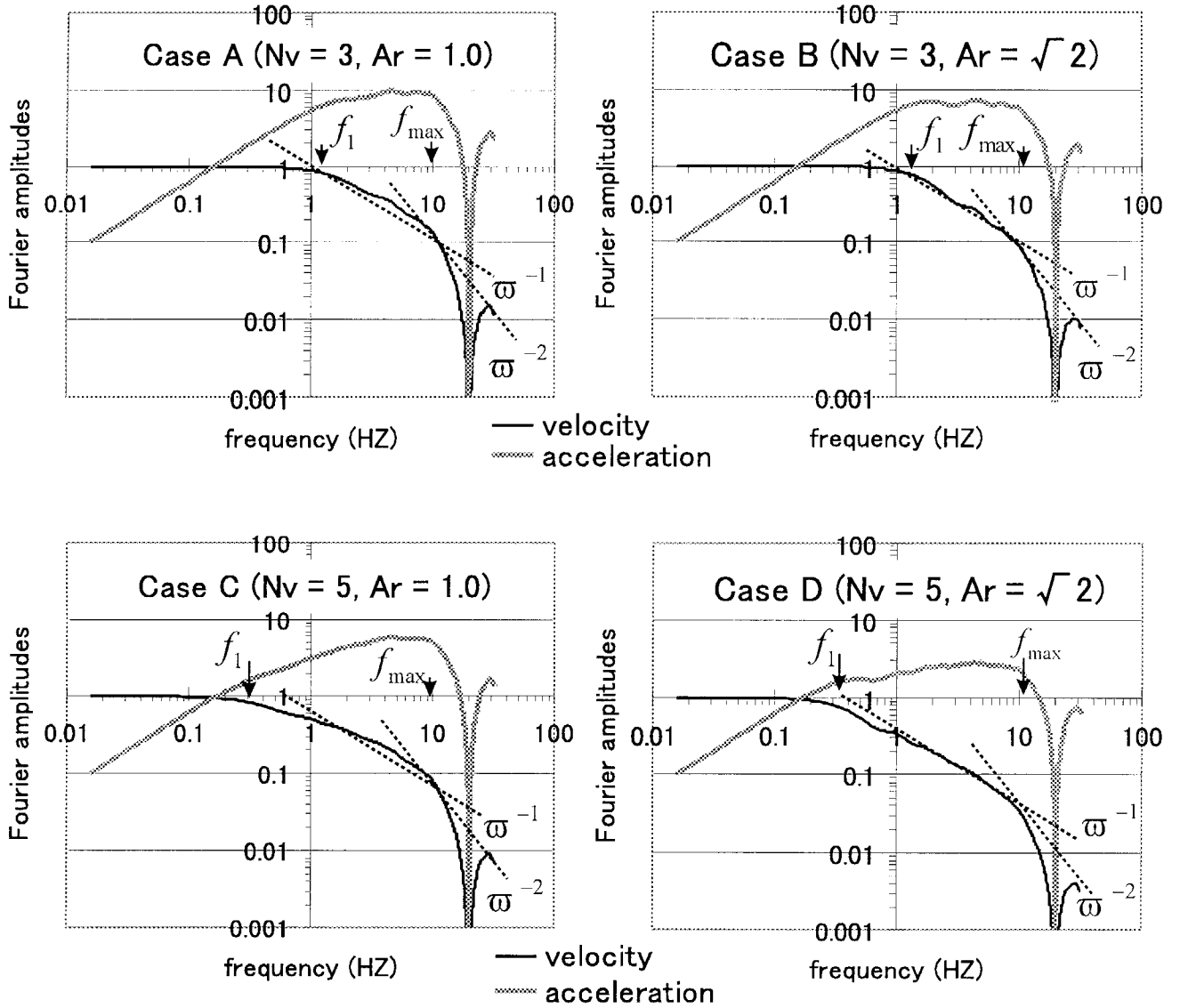
Figure 3.    The Fourier amplitude spectra of the slip velocities for the four cases shown in Figure 2. The Fourier spectra of the slip accelerations are also shown in gray lines. Note that the velocity spectra fall off as the inverse of $\omega$ between $f_1$ and $f_{max}$.

Here I use the simplest $k$-squared slip distribution, namely, the equilateral triangle,

$$D(x) = \begin{cases} 2D_m x/L, & (0 \leq x \leq L/2) \\ 2D_m(L - x)/L, & (L/2 \leq x \leq L) \end{cases} \quad (24)$$

where $D_m$ is the maximum slip at the center. For the constant rupture velocity ($\Delta t_r = 0$), the analytical solution can be obtained by substituting equation (24) into equation (23),

$$S(\omega) = \frac{LD_m}{2}\left\{\frac{\sin \chi_s}{\chi_s} e^{i\chi_s}\right\}^2 \quad \text{with } \chi_s = \frac{\omega L}{4\bar{V_r}C_d} \quad (25)$$

Note that the Fourier amplitude of equation (25) has the $\omega^{-2}$

decay at high frequencies; this would be the simplest $k$-squared model.

In order to evaluate equation (23) for $\Delta t_r \neq 0$, I subdivide the fault length $L$ into small segments $\Delta L_j$ (see Figure 1), and carry out the analytic integration on each subfault,

$$S(\omega) = \sum_{j=1}^{N_L} \int_{x_{j-1}}^{x_j} \bar{D}_j \exp\left\{i\omega\left(\frac{x}{\bar{V_r}C_d} + \Delta t_{rj}\right)\right\}dx,$$

$$= \sum_{j=1}^{N_L} \bar{D}_j \Delta L_j \frac{\sin \chi_j}{\chi_j} \exp\left\{i\omega\left(\frac{\bar{x}_j}{\bar{V_r}C_d} + \Delta t_{rj}\right)\right\}, \quad (26)$$

$$\text{with } \chi_j = \frac{\omega \Delta L_j}{2\bar{V_r}C_d}, \quad \text{and } \bar{x}_j = \frac{x_{j-1} + x_j}{2}. \quad (27)$$

where $N_L$ is the total number of subfaults. Note that the source spectrum $S$ is the superposition of the functions with the $\omega^{-1}$ decay.

As an example, I will use the following parameters to compute the source spectra up to 20 Hz: $L = 10$ (km), and $D_m = 1$ (m), $N_L = 2000$, $C_d = 1$, and $\overline{V}_r = 2.5$ (km/s).

First, I check the very basic effects of $\Delta t_r$ using the following two simple cases:

1. As shown in the left of Figure 4a, the rupture stops abruptly at the center of the fault for $\Delta t$ second, then continues to rupture. Thus, $\Delta t_r$ is expressed as,

$$\Delta t_r = \begin{cases} 0, & (0 \leq x \leq L/2) \\ \Delta t, & (L/2 \leq x \leq L) \end{cases} \quad (28a)$$

2. As shown in the right of Figure 4a, the rupture stops and starts two times. Thus, $\Delta t_r$ is expressed as,

$$\Delta t_r = \begin{cases} 0, & (0 \leq x \leq L/4, \text{ and } L/2 \leq x \leq 3L/4) \\ \Delta t, & (L/4 \leq x \leq L/2, \text{ and } 3L/4 \leq x \leq L) \end{cases} \quad (28b)$$

Figure 4b and 4c show the source spectra and their waveforms (i.e., the source time functions), respectively, for cases 1 and 2. The amplitudes of the source spectra are multiplied by $\omega$, and thus the constant amplitude represents the $\omega^{-1}$ decay. The source time functions in Figure 4c correspond to the displacement waveforms in the far-field. For reference, I plot the source spectra and the source time functions of the $k$-squared model using equation (25) by gray lines (Case 0; $\Delta t = 0$) in the figures. For Case 1, the abrupt stop at the center of the fault for $\Delta t$ second excites large high-frequency waves, and its spectrum shows the $\omega^{-1}$ decay with frequency. The source time function shows the extremely strong stopping phases, which seem unrealistic. Similarly, the spectrum for case 2 shows the $\omega^{-1}$ decay at high frequencies, but note that the maximum amplitudes are twice as large as those of case 1. The waveform shows the unrealistically strong stopping and starting phases at three locations. The abrupt stops and starts along the whole rupture front cause mathematical singularities and the results are physically unacceptable.

Next, I investigate the following more realistic three models considering smooth $\Delta t_r$ distributions: the $k$-inversed, $k$-squared, and $k$-cubed models.

*The k-inversed model for $\Delta t_r$.* The distribution of $\Delta t_r$ is assumed to be inversely proportional to the spatial wavenumber $k$. I construct this $k$-inversed model by superposing the cos functions, as follows.

$$\Delta t_r(x) = \sum_{m=1}^{M} \frac{\Delta t}{\sqrt{1 + m^2}} \cos\left(2\pi m \frac{x}{L} + \theta_m\right) \quad (28c)$$

where $\theta_m$ is a random phase between 0 and $2\pi$ (radians), $m$ is the wavenumber normalized by the fault length, and $M$ is the maximum value of $m$. $M\overline{V}_r/L$ gives the limit of resolution in frequency.

*The k-squared model for $\Delta t_r$.* The $\Delta t_r$ distribution is assumed to be inversely proportional to $k$-squared. Similar to the $k$-inversed model, I construct the model by superposing the cos functions, as follows.

$$\Delta t_r(x) = \sum_{m=1}^{M} \frac{\Delta t}{\sqrt{1 + m^4}} \cos\left(2\pi m \frac{x}{L} + \theta_m\right) \quad (28d)$$

*The k-cubed model for $\Delta t_r$.* The $\Delta t_r$ distribution is assumed to be inversely proportional to $k$-cubed. Similarly, I construct the model as follows.

$$\Delta t_r(x) = \sum_{m=1}^{M} \frac{\Delta t}{\sqrt{1 + m^6}} \cos\left(2\pi m \frac{x}{L} + \theta_m\right) \quad (28e)$$

Figure 5 shows the amplitudes of the $k$-inversed, $k$-squared, and $k$-cubed models by normalizing by $\Delta t$.

Figure 6a shows examples for $\Delta t_r$ distributions using the $k$-inversed, $k$-squared, and $k$-cubed models. I use $\Delta t = 0.1$(sec), which is 1/40 of the total duration ($L/\overline{V}_r = 4$ second), and $M = 500$ in equations (28c) to (28e), together with the same source parameters in cases 1 and 2. Figure 6b shows the source spectra corresponding to the three models in Figure 6a. Similarly to Figure 4b, the amplitudes of the source spectra are multiplied by $\omega$. The high-frequency amplitudes are nearly constant for the $k$-inversed model, fall off as the inverse of $\omega$ for the $k$-squared model, and fall off as the inverse of the $\omega$-squared for the $k$-cubed model. Figure 6c shows the source time functions for the three models. For reference, I plot the functions for $\Delta t = 0$ using equation (27) by gray lines in the figure. The waveform of the $k$-inverse model shows unrealistically strong and incoherent high-frequency waves; it is hard to identify the coherent waveform of the gray line. In contrast, the source time function for the $k$-squared model shows the high-frequency fluctuations around the coherent waveform, which seems realistic. The functions of the $k$-cubed model does not show incoherent high-frequency fluctuations; the smooth fluctuation corresponds to the *sin*-type $\Delta t$ seen in Figure 6a. Based on general expectations, the result of the $k$-squared model seems the most plausible.

Finally, I investigate the effect of $\Delta t_r$ on the $k$-squared model by changing the amplitude $\Delta t$ in equation (28d). Figure 7a shows the source spectra for $\Delta t = 0.1, 0.2, 0.4,$ and 0.8 seconds, which correspond to 1/40, 1/20, 1/10, and 1/5 of the total duration, respectively. The Fourier spectra increase with increasing $\Delta t$ at high frequencies, and show $\omega^{-1}$ decay except for $\Delta t = 0.8$. The high-frequency spectrum for $\Delta t = 0.8$ is independent of $\omega$. Figure 7b depicts the source time functions, which show the larger high-frequency fluc-
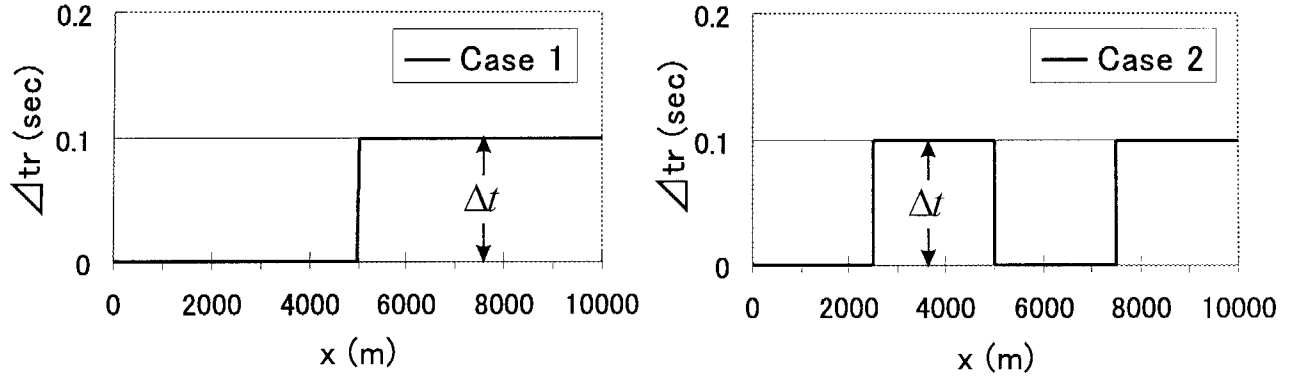
**(a) Distribution of the incoherent rupture time**
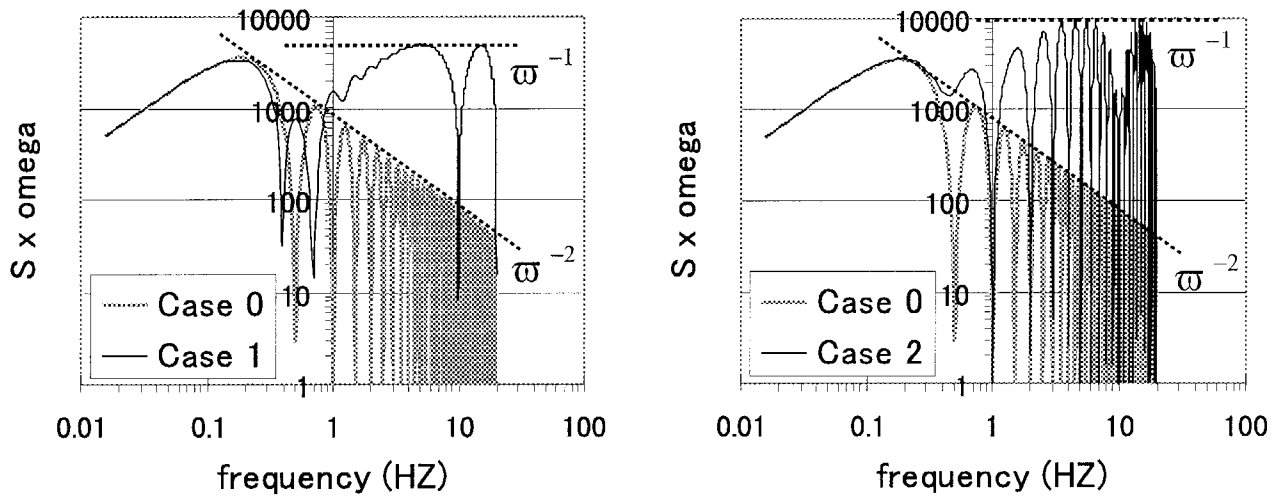


**(b) Source Spectra multiplied by omega**
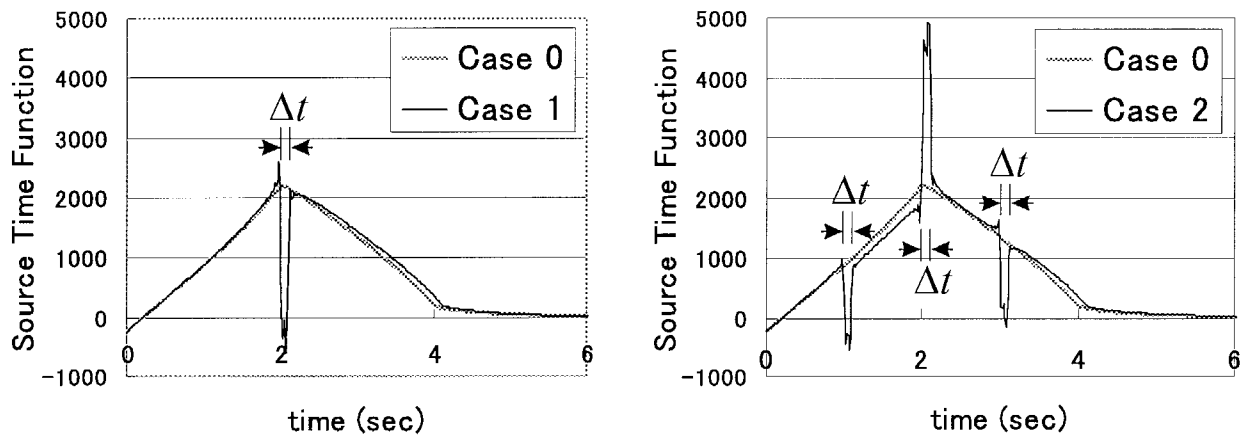


**(c) Source Time Functions**

Figure 4.    The incoherent rupture time $\Delta t_r$ for two cases (top), and their source spectra (middle) and corresponding source time functions (bottom). The rupture stops abruptly at the center of the fault for $\Delta t$ second for case 1, and the rupture stops and starts twice for case 2. The amplitudes of the source spectra are multiplied by $\omega$, and thus the constant amplitude represents the $\omega^{-1}$ decay. Gray lines indicate the case for the coherent rupture time (Case 0; $\Delta t = 0$).
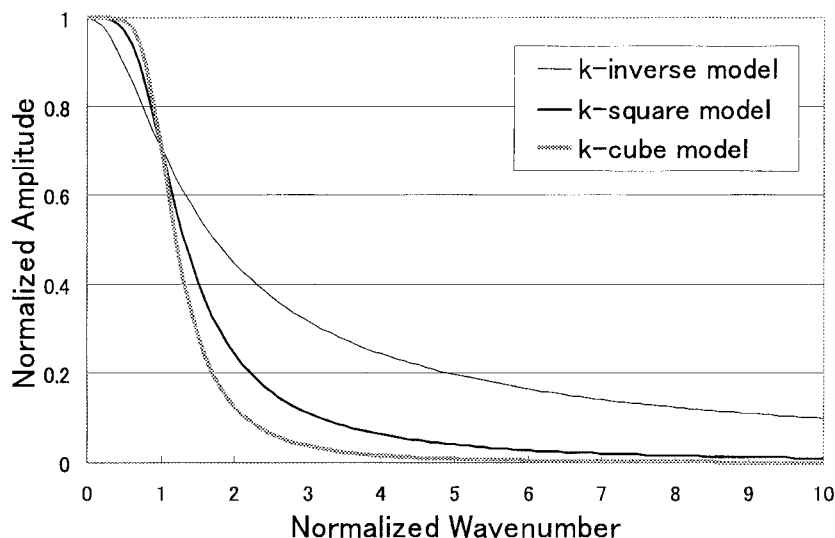
Figure 5. The normalized amplitudes of the *k*-inverse, *k*-square, and *k*-cube models for the $\Delta t_r$ distributions.

tuations for the larger $\Delta t$. In particular, the functions for $\Delta t = 0.4$ and $0.8$ show unacceptably incoherent fluctuations. Thus, a $\Delta t$ between $1/40$ and $1/20$ of the total duration may be appropriate.

## Discussion

From the results presented here, it appears that the most appropriate $\omega$-squared model consists of the slip-velocity model with *k*-squared spatial distributions in slip and incoherent rupture time, $\Delta t_r$. I call this model the $\omega$-inverse-squared model, because the $\omega$-squared source spectra consist of the two $\omega$-inverse models due to the slip velocity and the spatial variations, as discussed below.

Figure 8a and 8b shows schematic explanations for modeling the $\omega$-squared source spectra using the *k*-squared model of Bernard *et al.* (1996) and by the $\omega$-inverse-squared model, respectively. There are two main differences between the two models. The first is the modeling of slip velocity. The slip velocity of the former consists of the scale-dependent rectangular boxcars. In addition, this model allows the duration of boxcars to be infinitely small at the highest frequency; this is equivalent to the Dirac delta function, whose Fourier amplitude is constant with $\omega$. Consequently, the Fourier amplitude of the slip velocity becomes independent of $\omega$. On the other hand, the slip velocity of the $\omega$-inverse-squared model consists of triangles. As discussed earlier, the finite acceleration amplitudes of the triangles are physically more appropriate than the boxcars. In addition, this model introduces a minimum duration among the triangles, whose reciprocal represents the source-controlled $f_{max}$. Thus, the Fourier amplitude of our slip velocity model falls off as the inverse of $\omega$ up to $f_{max}$, and as the inverse of $\omega$-squared at frequencies higher than $f_{max}$. Even though it is still a matter for argument whether $f_{max}$ is caused by the source or site effects (Hanks, 1979, 1981; Anderson and Hough, 1984; Papageorgiou and Aki, 1985), it seems natural to have a corner

frequency controlled by smoothness in the slip velocity; otherwise the slip acceleration could be unacceptably large. The $\omega^{-1}$ decay of the source spectra of the slip velocity agrees with the empirical model derived by Dan and Sato (1999), although the latter is restricted to rather longer periods.

The other difference between the *k*-squared model and the $\omega$-inverse-squared model is the modeling of rupture velocity. The rupture velocity of the former is constant, whereas the latter is variable. As discussed earlier, the variable rupture velocity is more realistic, and it generates high-frequency waves efficiently. To model those effects, I introduced the incoherent rupture times $\Delta t_r$, and found that the *k*-squared model for $\Delta t_r$ distribution seemed the most plausible among the *k*-inversed, *k*-squared, and *k*-cubed models. The similar *k*-squared distributions for slip and $\Delta t_r$ may suggest some physical relationship between them.

As shown in the Figure 8b, the source spectrum of the $\omega$-inverse-squared model falls off as the inverse of $\omega$ under the assumption of the instantaneous slip (delta function as velocity) with the *k*-squared slip distributions. Since the source spectrum is expressed by the convolution of the slip velocity and the source spectrum with instantaneous slip, the source spectrum of this model falls off as the inverse of $\omega$-squared up to $f_{max}$ (namely, the $\omega$-squared model).

Finally, Figure 9 shows the comparison of source acceleration spectra among the *k*-squared model, the $\omega$-inverse-squared model, and an empirical $\omega$-squared model using the same source parameters in the previous section ($L = 10$ km, $D_m = 1$ m, $C_d = 1$, $N_L = 2000$, $\overline{V}_r = 2.5$ km/s, $M = 500$, and *fmax* $= 10$ Hz). All the spectra are normalized by the seismic moment. For the *k*-squared model, I use equations (13) and (15) with $a = 0.5$ and $L_0 = 0.2L$ (a broad-pulse model; Bernard *et al.*, 1996), whose corner frequency ($f_0 = a\overline{V}_r/L_0$) is 0.625 Hz. For the $\omega$-inverse-squared model, I show one example among many choices for the combinations for the slip velocities and the $\Delta t_r$ distributions, because the all results show similar $\omega$-squared source spec-
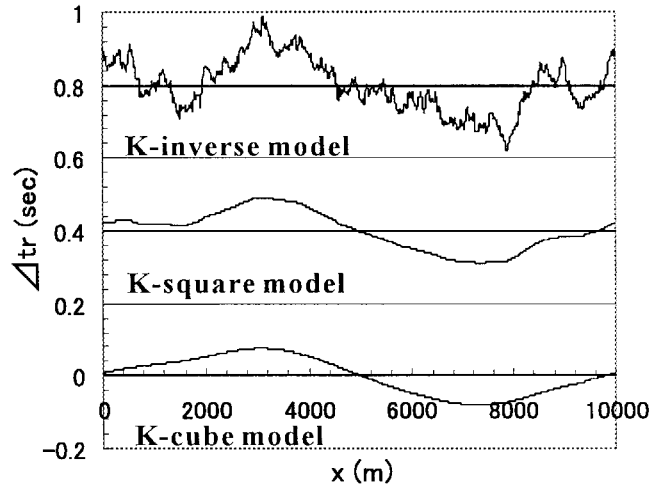
(a) Distribution of $\Delta t_r$
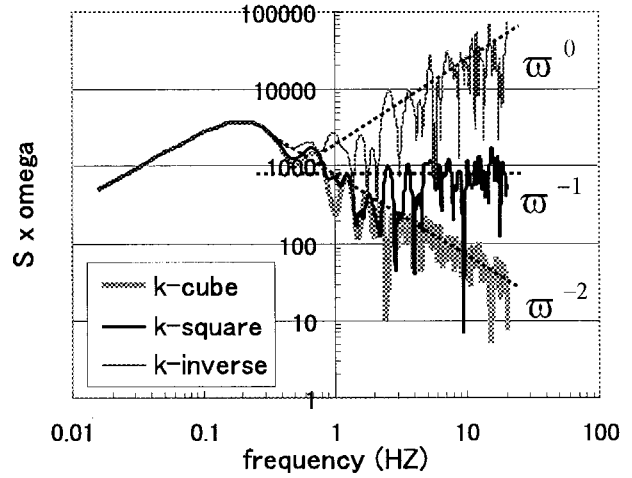
(b) Source Spectra x omega
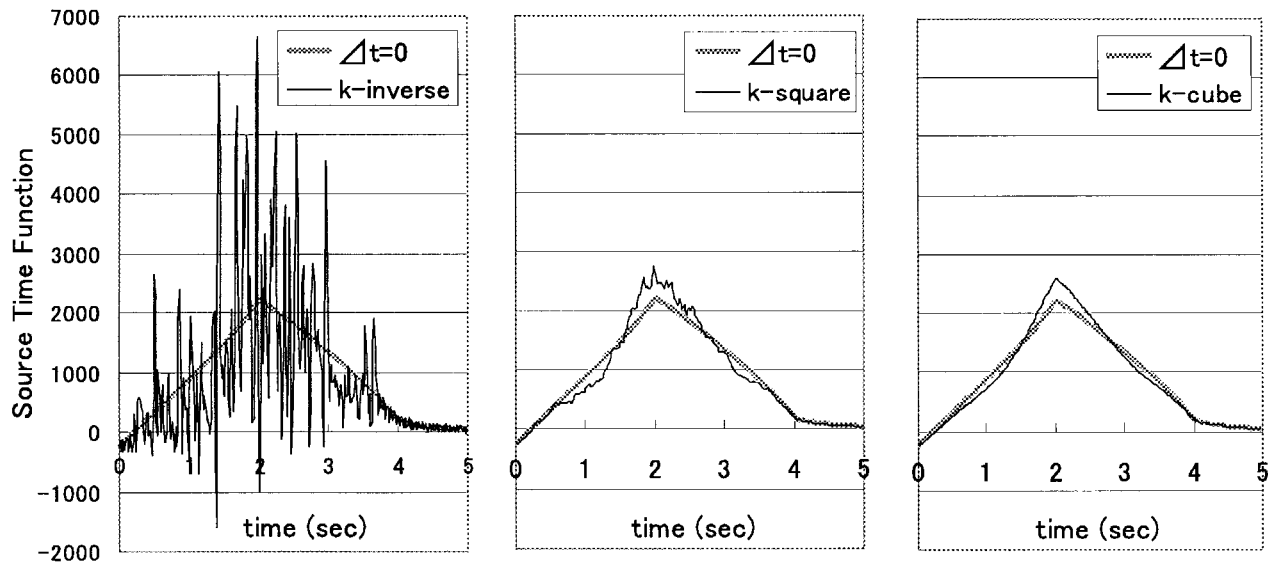


(c) Source Time Functions

Figure 6.    (a) The incoherent rupture time $\Delta t_r$ for the $k$-inversed, $k$-squared, and $k$-cubed models, and (b) their source spectra and (c) the source time functions. The amplitudes of the source spectra are multiplied by $\omega$, and gray lines indicate the case for the coherent rupture time ($\Delta t = 0$).

tra. The parameters for our model are $Ar = \sqrt{2}$, $N_r = 4$ ($\tau_{max} = 0.8$ sec and $f_1 = 0.63$ Hz), and $\Delta t = 0.2$ sec. As for the $k$-squared $\Delta t_r$ distributions, I generate one hundred sets of random phases in equation (28d), and show the average of source spectra with the standard deviations in the figure. For the empirical $\omega$-squared model, I use Brune's model (1970) with $f_{max} = 10$ Hz (Boore, 1983) and the corner frequencies $f_c = 0.147$ Hz (for $\Delta\sigma = 50$) and 0.234 Hz (for $\Delta\sigma = 200$) under the values of $W = L/2$, $Vs = 3.8$ km/sec, and $Mo = 1.01 \times 10^{26}$ dyne cm. As compared with Brune's model, the $k$-squared model and the $\omega$-inverse-

squared model show rather larger amplitudes at lower and higher frequencies, respectively. However, all the spectra shows similar $\omega$-squared amplitudes at high frequencies, overall.

In summary, I believe that no matter which models are used, the far-field acceleration waveforms would be similar. However, the broad-band strong motions, especially in near field, would be greatly different among the various models; the unphysical assumptions may cause implausible results. The advantage of the $\omega$-inverse-squared model is that it has a clear physical basis for the slip velocity and the spatial
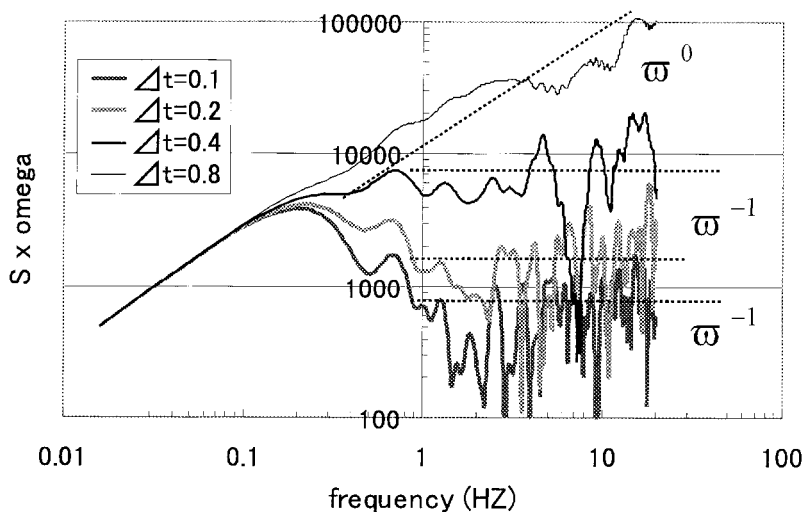
**(a) Source Spectra multiplied by omega**
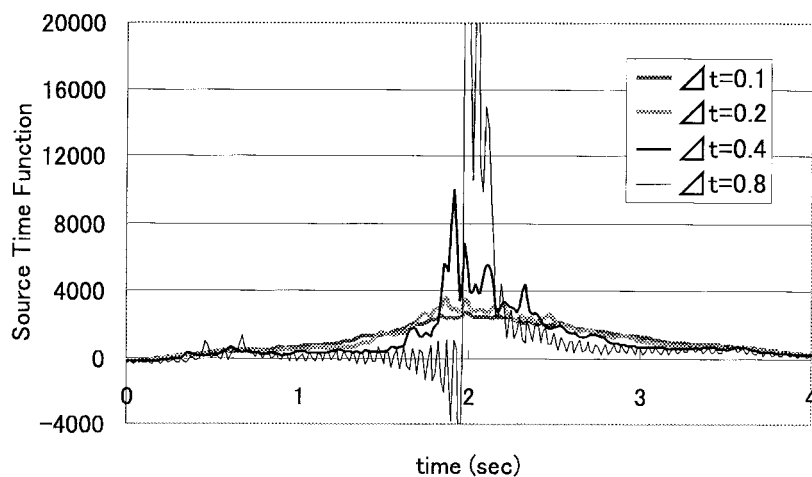


**(b) Waveforms of source spectra**

Figure 7. (a) The source spectra of the $k$-square models for $\Delta t_r$ for the cases of $\Delta t =$ 0.1, 0.2, 0.4, and 0.8 seconds, and (b) the corresponding source time functions. The amplitudes of the source spectra are multiplied by $\omega$.

variations in the slip and rupture time. This model could simulate the broadband strong motions from the near-field displacements (coherent and low-frequency waves) to the far-field accelerations (incoherent and high-frequency waves).

## Conclusions

I investigated the theoretical basis of the $\omega$-squared model by modifying the $k$-squared model of Bernard *et al.* (1996), and proposed the $\omega$-inverse-squared model by considering the spatial variation in slip distribution, slip velocity, and rupture velocity. For the slip velocity, I proposed a Kostrov-type model by superposing equilateral triangles, where the two corner frequencies are introduced. The first corner frequency $f_1$ corresponds to the slip duration, while the second is the source-controlled $f_{max}$. The Fourier ampli-

tude of this model falls off as the inverse of $\omega$ between $f_1$ and $f_{max}$. On the other hand, for modeling the effects of the spatial variation in rupture velocity, I introduced the incoherent rupture time ($\Delta t_r$), namely, the difference between the actual rupture time and the coherent (average) rupture time. After checking various models including the $k$-inversed, $k$-squared, and $k$-cubed distributions for $\Delta t_r$, I found that the $k$-squared model was the most plausible. I also found that its source spectrum fell off as the inverse of $\omega$, when the slip velocity is Delta function. Finally, I proposed the $\omega$-inverse-squared model, which consists of the combination of the slip velocity proposed earlier and the $k$-squared distributions in slip and $\Delta t_r$, and confirmed that it is consistent with the empirical $\omega$-squared models. Since this model provides the theoretical basis for constructing realistic source models at broadband frequencies, it would be useful for predicting strong ground motions including the near-field.
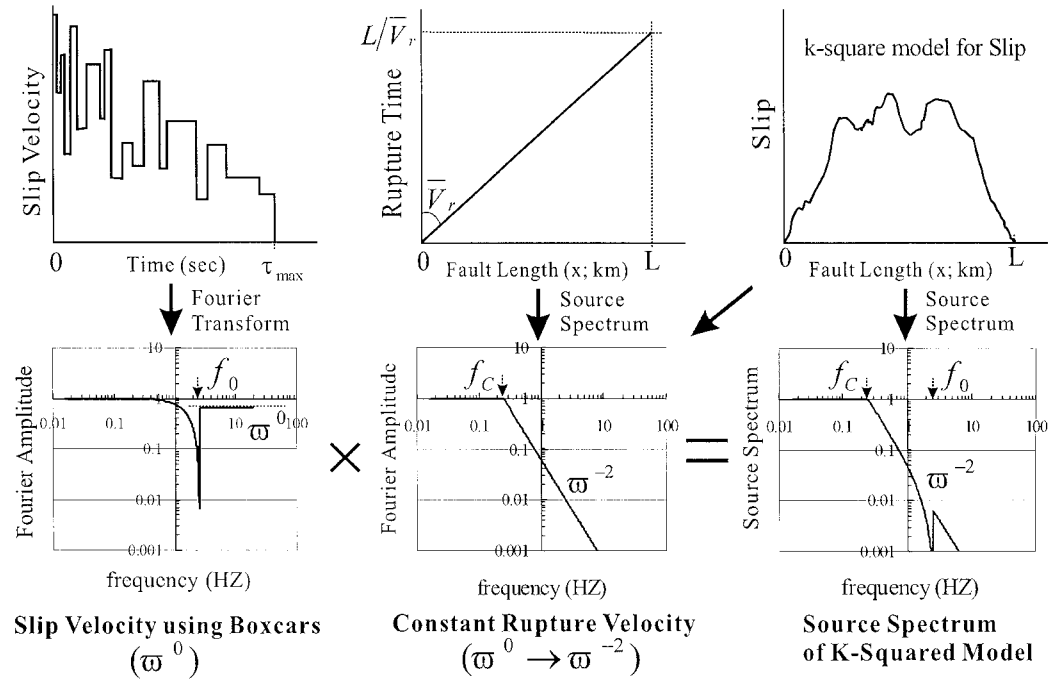
**(a) K-Squared Model**
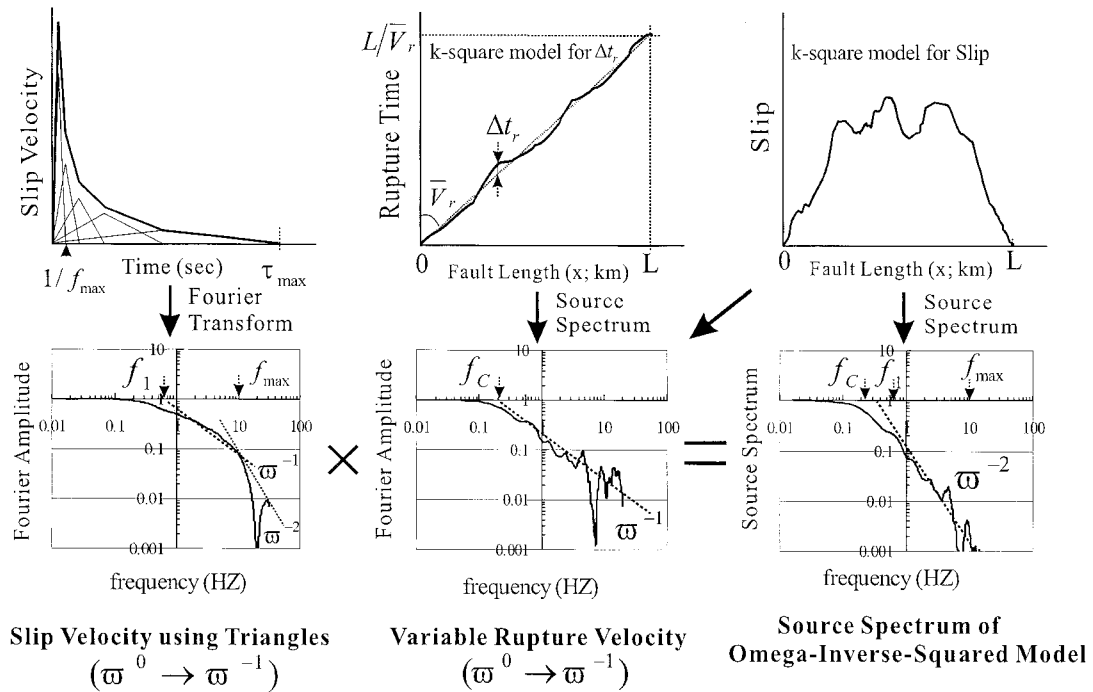


**(b) Omega-Inverse-Squared Model**

Figure 8.    Schematic explanations for modeling of the $\omega$-square model using (a) the $k$-square model (Bernard *et al.*, 1996) and (b) the $\omega$-inverse-squared model proposed in this article. The left figures in (a) and (b) illustrate the slip velocity models and their Fourier spectra. The middle figures show the modeling of rupture time, and their source spectra considering the $k$-squared slip distributions with the instantaneous slip. As shown in the bottom figures, the final source spectra are obtained by the convolutions of the slip velocity models and the source spectra with the instantaneous slip. Note that the $\omega$-inverse-squared model consists of the two $\omega$-inverse models.

**K-squared model**      **Omega-Inverse-squared model**
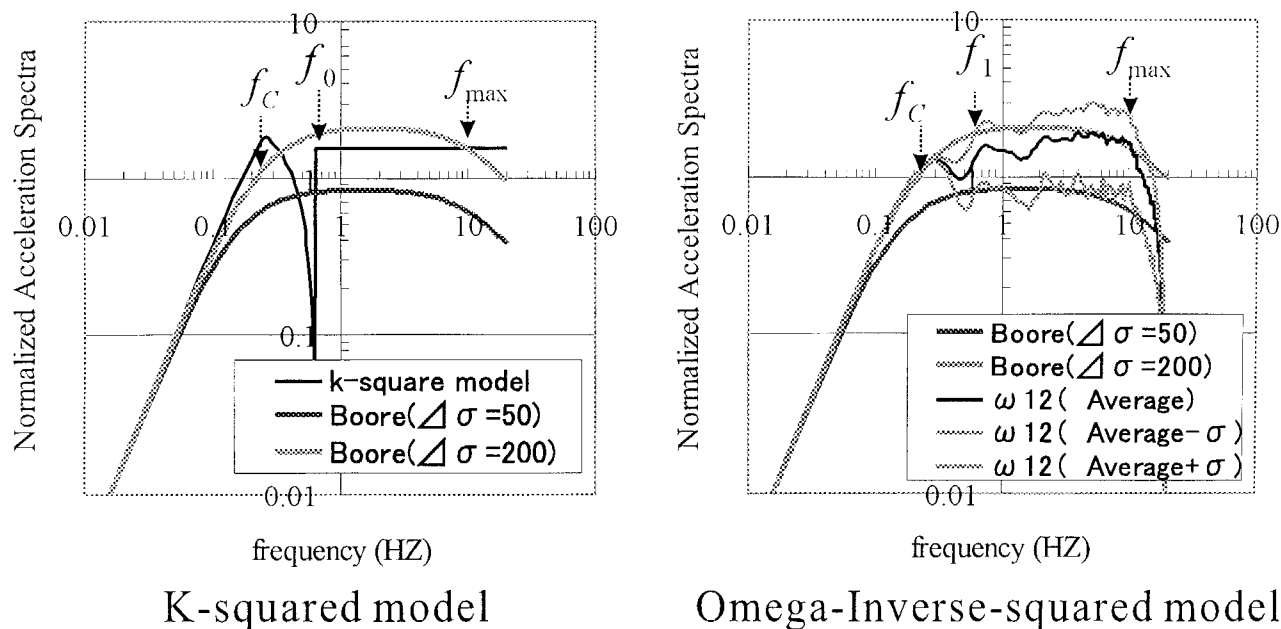
Figure 9. Comparisons of the acceleration source spectra among the *k*-square model, the $\omega$-inverse-squared model, and the empirical $\omega$-square model by Brune (1970) with $f_{max} = 10$ Hz (Boore, 1983). As for the $\omega$-inverse-squared model, the average value with the standard deviation are plotted using one hundred sets of random phases in equation (28d).

## Acknowledgments

## References

Aki, K. (1967). Scaling law of seismic spectrum, *J. Geophys. Res.* **72,** 1217–1231.

Aki, K. (1972). Scaling law of Earthquake Source Time-Function, *Geophys. J. R. Astr. Soc.* **31,** 3–25.

Andrews, D. I. (1981). A stochastic fault model, 2, Time-dependent case, *J. Geophys. Res.* **86,** 10821–10834.

Anderson, J. G., and S. E. Hough (1984). A model for the shape of the fourier amplitude spectrum of acceleration at high frequencies, *Bull. Seism. Soc. Am.* **74,** 1969–1993.

Archuleta, R. J. (1982). Analysis of near source station and dynamic measurements from the 1979 Imperial Valley earthquake, *Bull. Seism. Soc. Am.* **72,** 1927–1956.

Ben-Menahem, A. (1961). Radiation of seismic surface waves from finite moving sources, *Bull. Seism. Soc. Am.* **51,** 401–435.

Bernard, P., A. Herrero, and C. Berge (1996). Modeling directivity of heterogeneous earthquake ruptures, *Bull. Seism. Soc. Am.* **86,** 1149–1160.

Boatwright, J. (1982). A dynamic model for far-field acceleration, *Bull. Seism. Soc. Am.* **72,** 1049–1068.

Boore, D. M. (1983). Stochastic simulation of high-frequency ground motions based on seismological models of radiated spectra, *Bull. Seism. Soc. Am.* **73,** 1865–1894.

Brune, J. N. (1970). Tectonic stress and the spectra of seismic shear waves from earthquakes, *J. Geophys. Res.* **75,** 4997–5009.

Dan, K., and T. Sato (1999). A semi-empirical method for simulating strong motions based on variable-slip rupture models for large earthquakes, *Bull. Seism. Soc. Am.* **89,** 36–53.

Das, S., and K. Aki (1977). Fault plane with barriers: a versatile earthquake model, *Geophys. J. R. Astr. Soc.* **50,** 643–668.

Day, M. D. (1982). Three-dimensional finite difference simulation of fault dynamics: rectangular faults with fixed rupture velocity, *Bull. Seism. Soc. Am.* **72,** 705–727.

Frankel, A. (1991). High-frequency spectral falloff of earthquakes, fractal dimension of complex rupture, *b* value, and the scaling strength on fault, *J. Geophys. Res.* **96,** 6291–6302.

Gusev, A. A. (1983). Descriptive statistic model of earthquake source radiation and its application to an estimation of short-period strong motion, *Geophys. J. R. Astr. Soc.* **74,** 787–808.

Hanks, T. C. (1979). *b* value and $\omega^{-\gamma}$ seismic source models: implication for tectonic stress variations along active crustal fault zones and the estimation of high frequency strong ground motion, *J. Geophys. Res.* **84,** 2235–2242.

Hanks, T. C. (1982). *fmax, Bull. Seism. Soc. Am.* **72,** 1867–1879.

Hanks, T. C., and R. K. McGuire. (1981). The character of high-frequency strong ground motion, *Bull. Seism. Soc. Am.* **71,** 2071–2095.

Haskell, N. A. (1964). Total energy and energy spectral density of elastic wave radiation from propagating faults, *Bull. Seism. Soc. Am.* **54,** 1811–1841.

Heaton, T. H. (1990). Evidence for and implications of self-healing pulses of slip in earthquake rupture, *Phys. Earthq. Planet. Interiors* **64,** 1–20.

Herrero, A., and P. Bernard (1994). A kinematic self-similar rupture process for earthquake, *Bull. Seism. Soc. Am.* **84,** 1216–1228.

Irikura, K. (1986). Prediction of strong acceleration motions using empirical Green's function, *Proc. 7th Japan Earthq. Symp.* 151–156.

Joyner, W. (1984). A scaling law for the spectra of large earthquakes, *Bull. Seism. Soc. Am.* **74,** 1167–1188.

Kanamori, H., and G. Stewart. (1978). Seismological aspects of the Gua-temala earthquake of February 4, 1976, *J. Geophys. Res.* **83,** 3427–3434.

Koyama, J. (1985). Earthquake source time-function from coherent and incoherent rupture, *Tectonophysics* **118,** 227–242.

Kostrov, B. V. (1964). Self-similar problems of propagation of shear cracks, *J. Appl. Math. Mech.* **28,** 1077–1087.

Madariaga, R. (1976). Dynamics of expanding circular fault, *Bull. Seism. Soc. Am.* **66,** 639–666.

Madariaga, R. (1977). High-frequency radiation from crack (stress-drop) models of earthquake faulting, *Geophys. J. R. Astr. Soc.* **51,** 625–651.

Mikumo, T., and T. Miyatake (1978). Dynamic rupture process on a three-dimensional fault with non-uniform frictions and near-field seismic waves, *Geophys. J. R. Astr. Soc.* **54,** 417–438.

Miyatake, T. (1998). An approximate solution for slip rate and slip accel-eration time function in dynamic rupture propagation with slip weak-ening friction, *Proc. 3rd Symp. on Urban Disaster Mitigation for near Earthquake,* 67–68 (in Japanese).

Ohnaka, M., and Y. Kuwahara (1990). Characteristic features of local break-down near crack-tip in the transition zone from nucleation to dynamic rupture during stick-slip shear failure, *Tectonophysics* **175,** 197–220.

Papageorgiou, A. S., and K. Aki (1983). A specific barrier model for the quantitative description of inhomogeneous faulting and the prediction of strong ground motion, *Bull. Seism. Soc. Am.* **73,** 693–722.

Somerville, P., K. Irikura, R. Graves, S. Sawada, D. Wald, N. Abrahamson, Y. Iwasaki, T. Kagawa, N. Smith, and A. Kowada (1999). Charac-terizing crustal earthquake slip models for the prediction of strong motion, *Seism. Res. Lett.* **70,** 59–80.

Department of Architecture
Kogakuin University
Nishi-Shinjuku 1-24-2
Tokyo 163-8677, Japan
hisada@cc.kogakuin.ac.jp